Mon. Not. R. Astron. Soc. **359,** 315–327 (2005) doi:10.1111/j.1365-2966.2005.08898.x

A study of two post-common envelope binary systems

K. M. Exter,[1⋆†] D. L. Pollacco,[1] P. F. L. Maxted,[2] R. Napiwotzki[3] and S. A. Bell[4]

[1]*APS Division, Department of Pure and Applied Physics, Queen's University Belfast, Belfast BT7 1NN*
[2]*Astrophysics Group, School of Chemistry & Physics, Keele University, Staffordshire ST5 5BG*
[3]*Department of Physics and Astronomy, University of Leicester, University Rd, Leicester LE1 7RH*
[4]*HM Nautical Almanac Office, Space Science and Technology Department, Rutherford Appleton Laboratory, Chilton, Didcot*

Accepted 2005 February 1. Received 2005 January 27; in original form 2004 June 24

ABSTRACT

We present intermediate-resolution, phase-resolved spectra of the close-binary systems EC 11575−1845 and V664 Cas, the central star of the planetary nebula HFG 1. Both systems have a very rich emission-line spectrum originating from the face of the cool star, which is irradiated by the hot subdwarf star. The H I emission lines are wide, consistent with Stark broadening. These have a complex shape due to strong absorption near the line centre. We report on new spectroscopic orbits for both subdwarf stars, based on radial velocity measurements of their He II lines. The orbits of the heated face of the cool companions were measured from narrow emission lines, and from the wide H I profiles; some differences were found between ions. At phases around 0, absorption lines from the photosphere of the secondary star of V664 Cas are seen. These are used to estimate a spectral type of mid-F to early K, and we report on their radial velocities. Synthetic spectra from the non-local thermodynamic equilibrium model atmospheres were used to fit features in the optical spectrum of the hot subdwarf star of EC 11575−1845, from which we estimate $T_{\rm eff} = 105\,000 \pm 20\,000$ K, $\log g = 6.7 \pm 0.3$, $\log n_{\rm He}/n_{\rm H} = -0.8 \pm 0.1$. Finally, we consider the most likely range of component masses for these two systems.

Key words: binaries: close – binaries: spectroscopic – stars: individual: EC 11575−1845 – stars: individual: V664 Cas – subdwarfs.

1 INTRODUCTION

It is well known that the evolution of the components in binary systems with periods of a few hundred days or less is influenced by the nearby companion. During the primary's ascent of the asymptotic giant branch (AGB), the system will experience a common envelope phase where both components are engulfed by the primary's extended atmosphere (Iben & Livio 1993; Iben & Tutukov 1993). Viscous forces acting on the secondary will cause the orbit to shrink drastically; the orbital periods of these systems range from a few minutes up to a few days. The transfer of orbital angular momentum to the common envelope helps to expel it (e.g. Rasio & Livio 1996). As this material is mostly ejected in the orbital plane (Iben & Livio 1993), the energetic wind from the now exposed core of the primary most easily breaks out of the polar regions of the system. This is seen as a likely explanation for the formation of bipolar and axial-symmetric planetary nebulae (PNe; Mastrodemos & Morris 1999).

It is expected that an immediately post-common envelope binary (PCEB) system should appear as a hot subdwarf primary star and a late-type dwarf secondary star surrounded by a PN, and several such systems are currently known (Bond 2000). The two companions are in close proximity to each other and orbiting synchronously; they always have the same side facing each other. As a result of this, the high-energy photons from the primary star are absorbed in the facing atmosphere of the cool star. A characteristic of short-period PCEBs is therefore the reflection effect. This is a quasi-sinusoidal signal in the light curve with the same period as the binary orbit, and is caused by the increase in the flux when the heated face of the secondary star comes into view. In PCEBs with hot primaries [subdwarf O stars (sdO)], the amplitude of the reflection effect can be more than a magnitude at optical wavelengths. Emission lines are also produced, arising from the irradiated surface and moving in antiphase to the spectral lines from the primary star.

The structure of the atmosphere in the irradiated region of the secondary star is very different to that of a normal dwarf: as shown by Barman (2002), energy reprocessing occurs in the atmosphere. Thus, the algorithms used in numerical light-curve codes to deal with the reflection effect often break down in these cases of extreme irradiation. This typically results in light curves which can

⋆E-mail: katrina@ll.iac.es
†Current address: Inst. de Astrofísica de Canarias, c/Vía Láctea s/n, La Laguna, Tenerife, E38200, Spain.

only be modelled using albedos greater than unity (Drilling 1985; Pollacco & Bell 1993, 1994; Bell, Pollacco & Hilditch 1994).

An understanding of the physics involved in the energy reprocessing mechanism has proved elusive. Shimanskii et al. (2004) performed irradiation modelling on V664 Cas, fitting to the light curves and spectra, and although they do not give full details of the models, their results will be compared to ours in this paper. In the case of the binary BE UMa, which exhibits a large reflection effect, Ferguson & James (1994) attempted to model the upper regions of the affected atmosphere (where hydrogen is photoionized by the extreme ultraviolet flux from the primary), using the CLOUDY code (Ferland 1991). The model did not quite predict the observed emission-line spectrum (which is very similar to those presented here) but was successful in producing continuum variations similar to those observed. They predicted that a small ellipticity should be seen in the light curve directly as a consequence of the irradiation; a prediction that has not yet been tested. Pustylnik, Pustynski & Kubat (2001) also considered the ionization of hydrogen in the upper atmosphere of irradiated cool companions to hot subdwarfs. They found that the equilibrium temperature of the gas in these regions can be considerably higher than that expected using simple blackbody approximations. They suggested that this might be the basis of a rigorous method to determine the effective temperature of the subdwarf and of the irradiated region. Barman (2002) – see also Barman, Hauschildt & Allard (2004) – calculated model atmospheres for M dwarf companions in PCEBs, and fits to the H lines of the binary system GD 245 show that these models reproduce the irradiation effects well. He found that the radiation field from the white dwarf affects the atmosphere of the cooler star strongly, such that an irradiated atmosphere cannot be simply mimicked as a non-irradiated atmosphere of higher effective temperature. A large temperature inversion is set up in the upper atmosphere of the secondary star, one which is similar in appearance to a chromospheric transition region. The spectrum observed from this star will change with both phase and inclination, due to the varying amount of the irradiated face that is to view at each phase, as well as the different lines of sight to the irradiated gas (which exhibits a temperature gradient over the hemisphere).

In this paper we present intermediate-resolution, time-resolved spectroscopy of two PCEBs. In EC 11575−1845 the ejected nebula has not been detected, while the second, V664 Cas, is associated with a large nebula, HFG 1 (Heckathorn, Fesen & Gull 1982). Both systems have reflection effects with amplitudes $V > 1$ mag – among the largest known. The periods are 8 h (Chen et al. 1995) and 14 h (Grauer et al. 1987; Pigulski & Michalska 2002), respectively. We have used our emission-line spectra to improve on the Chen et al. (1995) model for EC 11575−1845 and to derive system parameters for V664 Cas for the first time. We also present a light curve for V664 Cas and the photospheric spectrum of the secondary star.

The observations and data reduction are described (Section 2), as are the details of the line measurements (Section 3), the absorption-line spectrum of the secondary star of V664 Cas (Section 4), the orbital solutions (Section 5), the analysis of the primary star parameters (Section 6), and calculations of the limits to the inclination and masses (Section 7). In Section 8 we discuss Stark broadening, and in Section 9 we summarize our results.

2 OBSERVATIONS AND DATA REDUCTION

EC 11575−1845 was observed on 1995 April 19 and 20 with the 3.5-m European Southern Observatory (ESO) New Technology Telescope at La Silla under remote control from Garching, Germany. The red optimized arm of the EMMI spectrograph was used with a 1200 l mm^{-1} grating and the 2048 × 2048 pixel Tektronix CCD giving a reciprocal dispersion of 13.5 Å mm^{-1} at the focal plane. We used a slit 1 arcsec wide to ensure radial velocity accuracy, and exposure times of 900 s. Our spectra cover the wavelength range 4270–4920 Å at a resolution of 1.1 Å. We obtained 23 spectra over several orbital cycles using the ephemeris of Chen et al. (1995) to ensure good orbital phase coverage. Each night was photometric with seeing around 1 arcsec. Observations were bracketed by exposures of a copper–argon source.

V664 Cas was observed with the double-beamed spectrograph ISIS at the 4.2-m William Herschel Telescope (WHT) on La Palma on 1994 December 20/21/23. Both arms utilized 1200 l mm^{-1} gratings giving a dispersion of 17 Å mm^{-1} on the 1024 × 1024 pixel Tektronix CCDs. This resulted in a resolution of 1.0 (blue) and 0.9 (red) Å and wavelength coverage of 4300–4720 and 6360–6760 Å. The atmospheric conditions were photometric with seeing of <1 arcsec, with the slit width matched to the seeing to ensure accurate radial velocity measurements. Exposures were 1200 s. Observations were obtained at both arms simultaneously using a dichroic mirror with a central wavelength of 5400 Å, and were bracketed by exposures of a copper–argon–neon source. There are 30 spectra covering most of the orbit. Two spectra were also taken of EC 11575−1845 with the same set-up and exposure times. Additional narrow slit observations of V664 Cas were taken for the purpose of creating an emission-line map, with the 600 (resolution ∼2 Å) and 1200 l mm^{-1} gratings and the same exposure times. The red-arm spectra were centred on seven different wavelengths from 5790 to 6800 Å over phases from 0.29 to 0.54. The blue-arm spectra were centred on seven wavelengths from 3750 to 5400 Å at the same phases.

The data were reduced using the software PAMELA and MOLLY (written by Tom Marsh[1]) and some standard Starlink[2] packages. The usual procedure was followed (bias subtraction, flat-field correction, sky subtraction, and then extraction of the target and arc spectra), with no flat-fielding for the ISIS spectra as there were features on the flat-field images obviously not on the astronomical images (this had an insignificant effect on the final spectra). The spectra were 'optimally extracted', i.e. with weights to give the maximum signal-to-noise ratio. No nebular lines were visible on the CCD images of V664 Cas. The wavelength calibration achieved rms residuals of 0.02–0.04 Å for the higher-resolution spectra and 0.03–0.07 Å for the lower-resolution spectra. The spectra were then divided by a low-order polynomial fit to the continuum and binned to a uniform velocity scale. The data were taken as part of a radial velocity study; thus, no flux calibration was carried out and no spectral-type standards observed.

Photometric observations of the V664 Cas field were obtained with the 1.0-m Jacobian Kapteyn Telescope (JKT), La Palma, on 1994 November 12–14 using a 1024 × 1024 pixel Tektronic CCD with Harris V and I filters and 100-s exposures. We used the IMRED packages within the IRAF environment (Tody 1993) to subtract the bias level and apply a flat-field correction to the images. Differential magnitudes in the instrumental system for V664 Cas and three comparison stars were measured with the APPHOT package. A combined differential magnitude was formed from the counts from each comparison star. No attempt was made to correct for airmass and colour effects.

[1] See http://quetzel.csc.warwick.ac.uk/phsaap/software

[2] See http://star-www.rl.ac.uk.

3 FITTING THE SPECTRAL LINES

The spectra of both binaries consist of absorption lines from the primary star – and for V664 Cas also from the secondary star – and emission lines from the irradiated face of the secondary star. A consequence of irradiation is that when the heated face of the secondary star comes into view, the continuum level of the combined spectrum increases and the irradiation-induced emission lines are at their strongest. The resulting orbital variations to these spectra can be seen. Fig. 1 includes an example of EC 11575−1845 at phase $\Phi \sim 0$, when the heated hemisphere is pointing away from us, to reveal the spectrum of the primary star, and at $\Phi \sim 0.5$, showing the irradiated face of the secondary star and its consequent emission lines. V664 Cas varies relatively little in its spectrum with phase, a consequence, most likely, of a low inclination and/or a large irradiated 'spot'. The red and blue spectra at ∼0.5 only are included in Fig. 1.

The radial velocities of the spectral lines also vary with orbital phase, those from the primary and secondary star moving in antiphase to each other. The absorption lines from the primary star measure the motion of its centre of mass, as they arise evenly from the photosphere over the whole star. However, the emission lines from the secondary star arise only from the irradiated face, and thus their velocity variations are biased to that side of the star. They measure rather the motion of the centre-of-light of the heated area. For the same reason, the photospheric absorption lines from the secondary star, visible at phases around 0, may also be biased to the unaffected side of the star; the spectrum that would arise from the heated side will be significantly quenched by the effects of the incoming flux from the sdO star. This is discussed again in Section 4.

Gaussian profile fitting was used to measure the radial velocities of the various emission lines, as the complex nature of the spectra, especially for He II and H I, make this procedure simpler than the alternative of cross-correlation with template spectra. We did compare the Gaussian fit results with cross-correlation results for the isolated emission lines; the derived K values the same to within their errors. For measuring the radial velocities of the absorption spectrum from the secondary star of V664 Cas, the low signal-to-noise ratio of the individual lines made cross-correlation a more attractive option.

3.1 He II 4686 Å

The He II profile of EC 11575−1845 (Fig. 1) consists of the absorption from the primary star, which has an emission peak in the core (typical for hot degenerate stars), and emission from the secondary star. The emission components were fit by least-squares with single

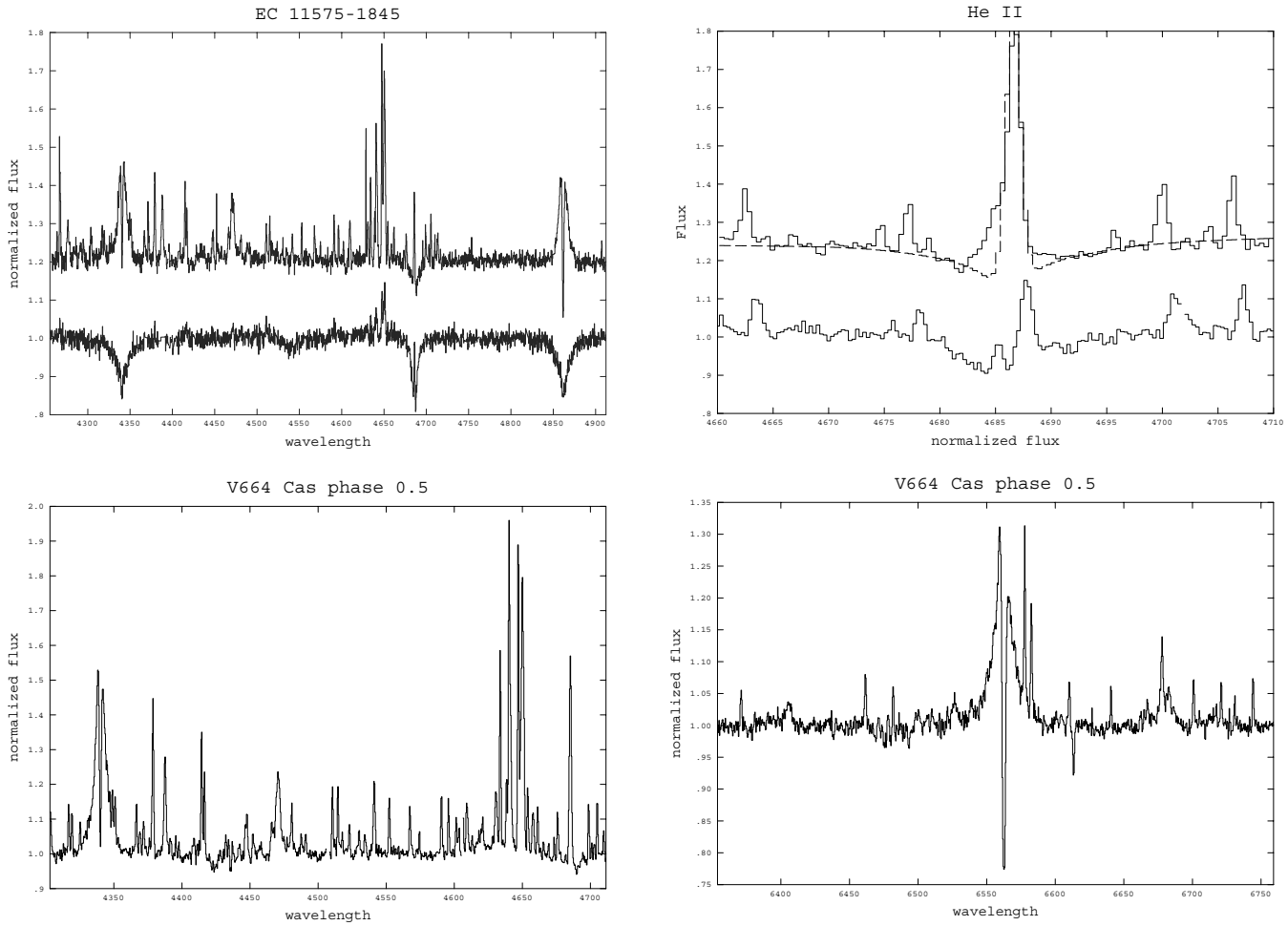

Figure 1. Top left: EC 11575−1845 at $\Phi = 0$ (lower) and 0.5 (upper). Top right: He II profiles. For EC 11575−1845 we see an absorption+emission line from the primary star and a redward-shifted emission line from the secondary star. For V664 Cas similar is found; however, to reveal the emission from the primary star, its absorption line and the secondary star's emission line were fit, as shown, and then subtracted. Bottom row: blue and red spectra of V664 Cas at $\Phi = 0.5$. All spectra have been continuum divided and plotted on an arbitrary scale.

Gaussian profiles, the wide absorption line with two profiles (set to the same wavelength) with the emission and absorption components from the primary constrained to the same radial velocity.

In the case of V664 Cas, the combined profile is similar to that for EC 11575−1845; however, here the secondary's emission line is blended with that from the primary star. It appears as a red or blue wing, at opposite quadratures, to the larger He II emission line. The absorption and secondary's emission line were fit with Gaussian profiles, the latter by eye to the core and the unaffected side. These were subtracted from the data, to reveal the residual emission line from the hot star, which was then fit with a Gaussian profile.

3.2 H I

The H I emission lines from the secondary stars are wide, peaking at ∼800 km s^{-1} full width at half-maximum (FWHM). All H I profiles have an absorption line located either at the line centre (V664 Cas) or such that it switches sides with phase (EC 11575−1845); see Fig. 2. For the Hα line of V664 Cas, the absorption appears to split into two at phases around 0. In all cases, the H I radial velocities follow that of the other emission lines on the spectra, and therefore are associated with the secondary not the primary star.

Two Gaussian profiles fixed to the same radial velocity were used to fit the H I emission lines, and one for the absorption component of EC 11575−1845 and for Hγ of V664 Cas. Two Gaussian profiles, separated by 80 km s^{-1}, were adopted for the absorption at Hα for V664 Cas; although the absorption profile is only seen with two cores at phases around 0, these fits gave the lowest errors for all phases. The resulting radial velocity solution differs from that determined from single-Gaussian absorption fits only in the value of the systemic velocity, γ (Section 4). For both systems, the absorption from the primary star, visible around $\Phi = 0$, was fit only to remove it, being of insufficient quality for any velocity determinations. Initial parameters were determined from Gaussian profiles fit separately to the emission and absorption components of the H I lines.

3.3 Narrow lines

All other lines of narrow width, mainly from permitted transitions of C, N and O, which were of adequate signal-to-noise to follow over most of the orbit, were fit with single Gaussian profiles. The initial ion identifications were taken from the work of Ferguson & James (1994) on BE UMa, and by selecting the ions that lie closest to the wavelength of the lines in question (using the line list of P. van Hoof on http://www.pa.uky.edu/∼peter/atomic/). Affirmation of the identifications came from a match for the value of γ to that determined from the unambiguously identified ions He II 4686 Å, or C II 6578 and 6583 Å, resulting in an uncertainty to the identification of ±3 km s^{-1}.

The lines with ion identifications are given at the end of Table 1. Multiple transitions have been wavelength averaged and are quoted within brackets, ⟨ ⟩.

4 SECONDARY STAR OF V664 CAS

On the red spectra of V664 Cas, there are faint but clearly present photospheric absorption lines, which move with the emission lines from the secondary star, as shown on the grey-scale trail plot of Fig. 3. The strongest of these lines are visible over much of the orbit, fading at phases around 0.5 and most prominent between $\Phi = 0.7$ and 0.2, i.e. when the cool hemisphere of the secondary star faces us. The radial velocity corrected and summed spectrum of this cool side is shown in Fig. 3. Comparison to a template of $T_{\rm eff} =$ 5300 K, $\log g = 4.5$, kindly provided by Barry Smalley (University of Keele), suggested identification of the most prominent lines with Fe I (our lines at ∼6400, 6496 Å), Ca I (∼6439, 6450, 6492 Å) and Ba II (∼6496 Å). Gaussian fits to these lines have a FWHM of 45 ± 13 km s^{-1}, close to resolution of the spectra. The absorption line at ∼6614 Å shows no radial velocity variations and is very close to an interstellar diffuse band identified by Jenniskens & Desert (1994). We have assumed that the secondary star is a dwarf, as no features expected from a giant star are found (and similarly for EC 11575−1845).

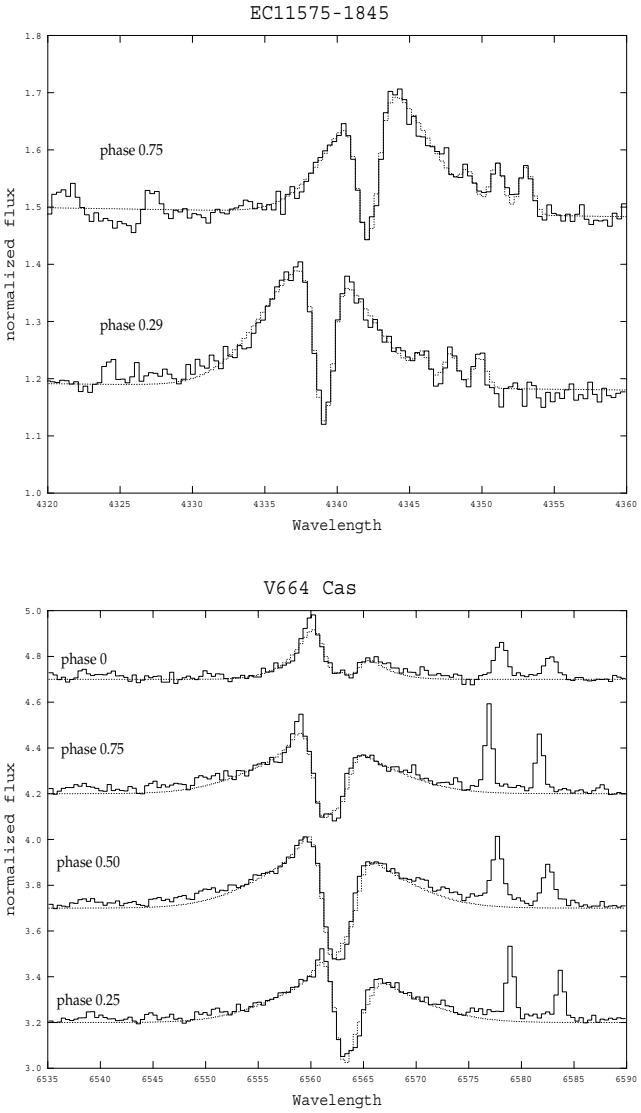

Figure 2. Top: Hγ and fits for EC 11575−1845 at Φ 0.25 and 0.75, showing the difference in the position of the emission and absorption components at these phases of maximum radial velocity. Bottom: the Hα line and fits for V664 Cas, at phases spread evenly over the orbit. Here one can see that for $\Phi = 0$ the absorption is very significant. It also appears that at phases between $\Phi = 0.75$ and 0, the absorption is separated into two components.

At He I 6678 Å, as can be seen from Fig. 3, there appears to be absorption structure similar to that for the H I lines. However, fitting this line as such results in a value of the systemic velocity some 100 km^{-1} different to that obtained from the other lines on the spectra. It is therefore more likely to be a region of blended lines.

Table 1. The derived orbital parameters for V664 Cas and EC 11575−1845 with their 1σ errors. All results are from the Gaussian fitting technique except for the 'absorption' entry of the secondary of V664 Cas, which is from cross-correlation. Periods were taken from the light curves, and errors are given in brackets. No errors means uncertain values.

	V664 Cas		EC 11575−1845	
Line	γ (km s^{-1})	K (km s^{-1})	γ (km s^{-1})	K (km s^{-1})
		SECONDARY		
Absorption		76(8)		
He II[a]	−10(3)	65(2)	10(2)	131(3)
He I[b]	−2(2)	59(2)		
		EMISSION LINES		
Blue	−5(2)	61(2)[c]	11(2)	124(2)[d]
Red[e]	−5(2)	46(2)		
Hγ		69(10)		211(10)
Hβ				209(5)
Hα		56(7)		
		H I ABSORPTION LINES		
Hγ	−5	62(17)	11(2)	122(5)
Hβ			16(2)	127(5)
Hα		53(7)		
		PRIMARY		
He II	−5(5)	74 (49-89)[f]	18(2)	53(2)
		T_0 **(HJD) + P (d)**		
	244 9708.410(1)+0.5817(2)		244 9827.6097(5)+0.32762(3)	

[a]4685.71 Å.
[b]6678.1517 Å.
[c]O II 4416.975 Å, N III ⟨ 4510.92 Å⟩, C III 4647.419 Å, N III 4634.12 Å.
[d]Same as [c] but C II ⟨ 4267.148 Å⟩ instead of N III 4510 Å.
[e]C II 6578.05, 6582.88 Å, O II 6641.031, 6721.387, N II 6482.01, 6701.22 Å.
[f]See Section 5.1.

4.1 Spectral type

An average of the V664 Cas spectra at phases around 0, with the emission lines removed, allowed for an estimate of the spectral type of the secondary star. As comparison templates, stars of type F5 V to M1.5 V were taken from the data base of Montes, Ramsey & Welty (1999). They were convolved with a Gaussian of FWHM of 45 km s^{-1}, velocity binned as were the V664 Cas red spectra, and wavelength shifted to match the position of Hα on our $\Phi = 0$ spectrum. They were then continuum diluted until the absorption lines matched the depths of those visible on V664 Cas spectra; the best value for the dilution was found by χ^2 minimization.

Our resolution is low enough that, combined with coincidences between secondary star absorption and emission-line features, we can only constrain the spectral type to a range F5–K5 V. Close inspection of individual lines by eye (the χ^2 values being similar for all) leads to the range F5–late G/early K. It should be noted that the spectrum of the secondary star may not reflect its true spectral type (or rather, its mass) as (i) our dilution is a simplification of the true additional continuum contributions from the irradiated region and the primary star, and (ii) it may be that energy is transported from the irradiated side to the unirradiated side (Beer & Podsiadlowski 2002).

International Ultraviolet Explorer (*IUE*) spectra SWP32090 and LWP11876 were extracted from the Multimission Archive at the Space Telescope Science Institute (MAST)[3] web site and merged by ourselves. The data were dereddened using the Seaton (1979) law with $R = 3.1$, until the 2200-Å interstellar absorption feature was flattened, resulting in $E(B–V) \sim 0.5$. The phased magnitudes of V664 Cas (both stars) at any wavelength are not recorded in the literature, so we adopt the catalogue value from Acker et al. (1992) of $V = 13.4$, and we set $R = V$. Assuming an equal magnitude for the primary and secondary in the R band (as the secondary spectrum is visible, they must be at least comparable), this leads to $R \sim 14.5$ for the secondary star. Assuming a spectral type range of F5–K0 V, a distance to the PN of 950–310 pc can therefore be derived. Heckathorn et al. (1982) have found the Shklovsky statistical method [constant F($H\beta$)] implies a distance of around 400 pc assuming a reddening of $E(B–V) = 0.43$ (derived from early-type stars in this galactic sightline). At our range of distance, a diameter for the nebula HFG 1 of 500 arcsec and expansion velocity of 15 km s^{-1} (Acker et al. 1992) lead to an expansion age range of 25–75 $\times$ 10^4 yr; the upper limit, especially, is very old for a PN.

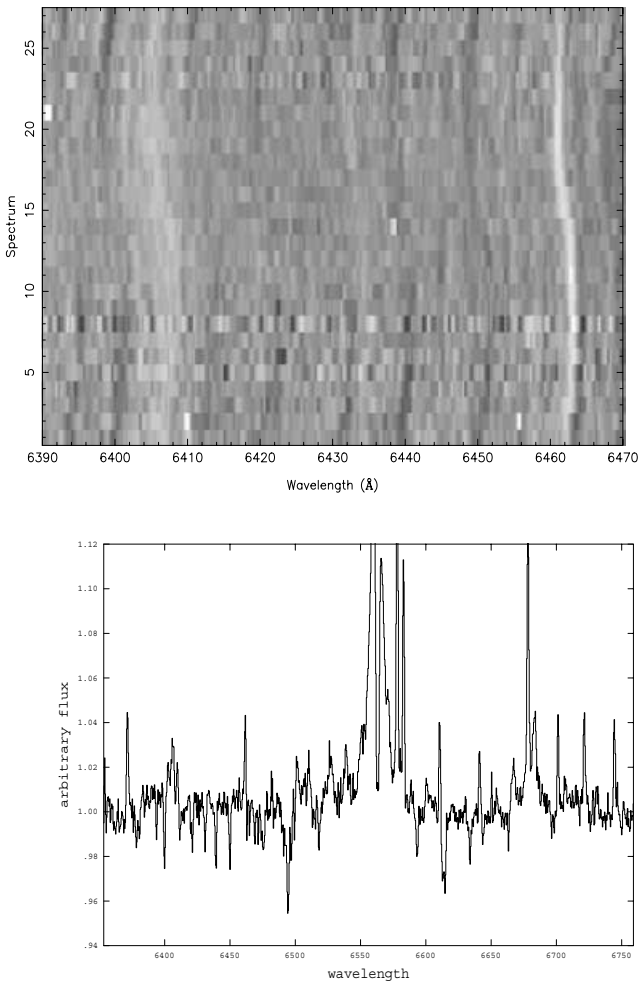

Figure 3. Top: trailed spectrum of the absorption lines (dark) from the secondary star of V664 Cas showing that their motion is synchronous with the emission lines (bright). Bottom: radial velocity corrected and summed spectrum showing the photospheric lines from the secondary component of V664 Cas.

4.1.1 Fitting the secondary spectrum

We used the cross-correlation method to measure the radial velocities of the absorption lines of the secondary star of V664 Cas.

[3] See http://archive.stsci.edu/.

Main-sequence template standard stars from Prugniel & Soubiran (2001) of types G6, G8, K3 and K5 were used for the cross-correlation against V664 Cas, with very similar results in all cases. The template spectra were broadened in MOLLY by blurring with a Gaussian profile of velocity FWHM 45 km s^{-1} and binned to the same scale as V664 Cas. The lines also were diluted to match the depths of those on our observed spectra. The most prominent emission lines were then snipped out of the V664 Cas spectra, and the FIGARO procedure SCROSS was carried out in the wavelength region 6385–6510 Å.

As the emission-line velocities were derived from Gaussian profile fits, we compared the results of these cross-correlations with Gaussian fits for the absorption spectra. Gaussian profiles were fit to the most prominent absorption lines, at ∼6400, ∼6440 and 6495 Å (the latter in fact being a complex of lines). To improve the signal-to-noise, the spectra were binned in pairs, resulting in a phase resolution of 0.1. These results were not used in our subsequent analysis as they cover a smaller range of phases than the cross-correlation analysis. The K value, 68 ± 6 km s^{-1}, is smaller but within the error the same as that eventually adopted.

As pointed out previously, the photospheric absorption lines from a star normally measure the motion of its centre of mass. Our absorption lines are however significantly quenched on the irradiated face of the star; there is therefore almost no contribution to the line profiles from this side. This could lead to the measured velocities being biased towards the unirradiated side, which, being located further away from the centre of mass of the system than the centre of mass of the (whole) secondary star, would result in larger measured velocities. The extent of this would depend on the relative sizes and luminosities of the irradiated and unirradiated faces, details we found we could not limit from our current data set, as we could not place tight enough limits on the size of the star and inclination of the system. We are however currently computing full irradiation models of both binary systems (see, for example, Exter et al. 2005), based on the work of Barman et al. (2004). Therefore, no correction has been made in this current analysis.

5 ORBITAL SOLUTIONS

The Gaussian fits yielded, for each line of each spectrum, the heliocentric-corrected velocity. These radial velocities, V, were then fit with a sine curve (i.e. assuming a circular orbit) using

$$V = \gamma + K \sin \frac{2\pi}{P}(T - T_0)$$

to determine γ, the systemic velocity, P, the period, K, the semi-amplitude, and T_0(HJD) the time of minimum light, for each line. The cross-correlation velocities were also fit, yielding one value of V for the whole spectrum.

The initial values of T_0 and P were taken from Chen et al. (1995) for EC 11575−1845 and from our ephemeris for V664 Cas (Section 5.3). The values of T_0, P, γ and K were first varied as free parameters, with optimization via least-squares fitting. For both systems, the periods derived from their radial velocity variation are, within the errors, in good agreement with those from the light curves. As the periods derived from the light-curve fitting have lower formal errors, these were used in the subsequent analysis. The final values of T_0 were taken from the fits to the narrow emission lines.

Table 1 lists the values of K and γ calculated from the sine fits, for various spectral features (we have only included those with reasonable errors). The radial velocity curves for the narrow lines were fit together to produce the orbital solutions; these are the 'red' and 'blue' entries of Table 1. For He I 6678 Å for V664 Cas, a double sine curve gave the best fit

$$A + B \sin\theta + C \sin 2\theta$$

where A is γ and B is K. There is little difference in the values of A and γ, B and K with that from a single sine curve, and $C/B = -0.10 \pm 0.02$. Radial velocity curves for V664 Cas are shown in Fig. 4, and for EC 11575−1545 in Fig. 5.

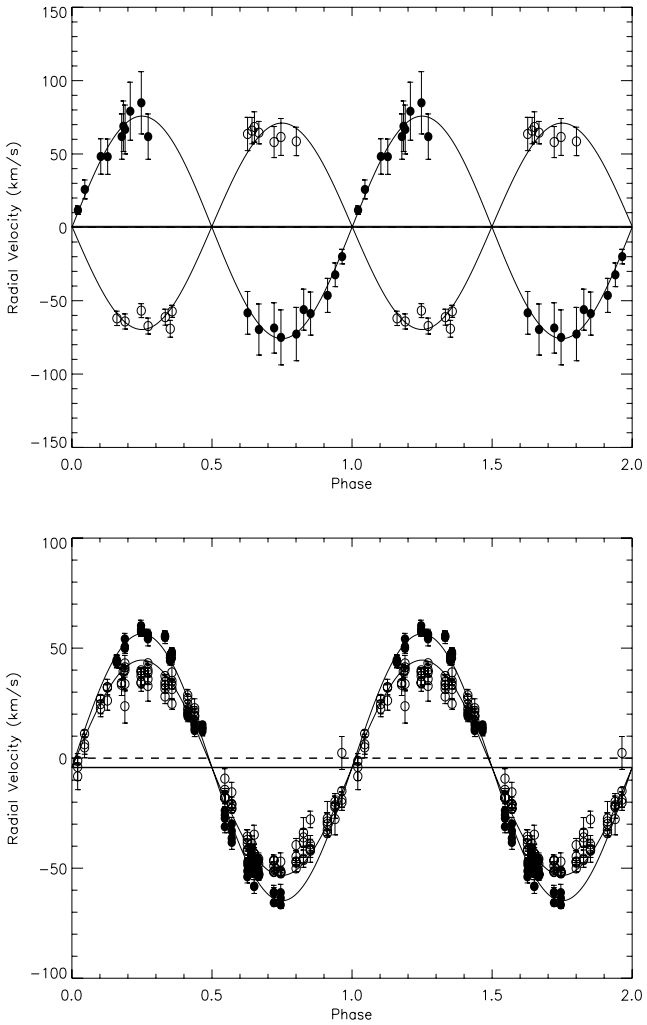

Figure 4. Top: the radial velocities and sine fit for the photospheric lines of the secondary component (filled symbols) and for He II from the primary (unfilled symbols) component of V664 Cas. Bottom: radial velocities and fits for the blue (filled) and red (unfilled) emission lines of V664 Cas.

5.1 V664 Cas

The spectra of V664 Cas provided a few puzzles. The first is that for the blue spectra of night 2, taken between phases 0.82 and 1.15, the radial velocities are conspicuously slower by about 30 km s^{-1} compared to the other nights (i.e. they are of lower absolute value when at phases such that they are both $>\gamma$ and $<\gamma$). The few overlapping phase points show the jump in velocity is only for night 2. We could not find any source for this in the data reduction or observing set-up; the arcs and sky spectra showed no such effect. However, it is not seen in the red spectra, and there are no accompanying changes to the line fluxes or line ratios. We therefore suspect it is not intrinsic

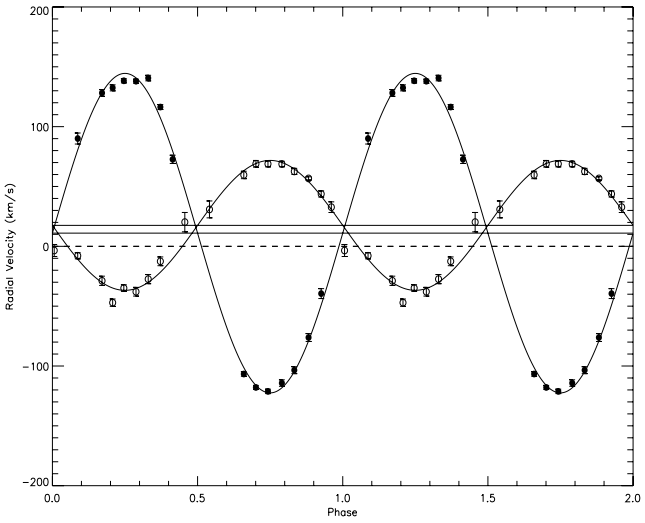

Figure 5. He II radial velocities and sine fit for EC 11575−1845, with the secondary star emission-line data plotted as filled symbols, and the primary star data plotted as unfilled symbols.

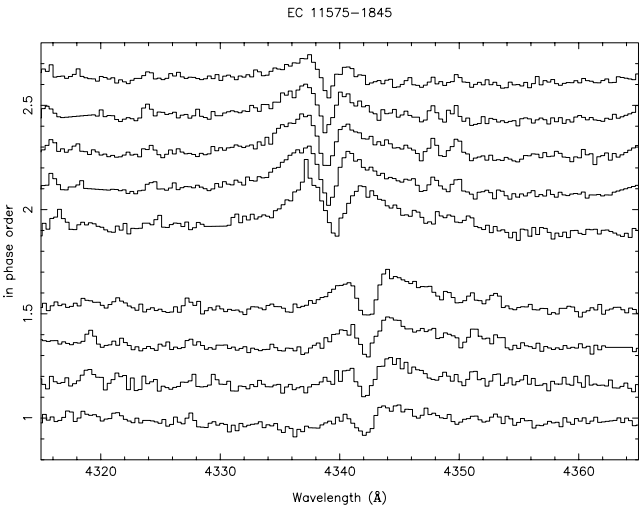

Figure 6. Spectrum of the Hγ line of EC 11575−1845 at phases around 0.25 (bottom four) and 0.75 (top four).

to the binary, but rather to the instrument, so the night 2 blue spectra are excluded from the radial velocity study.

The second puzzle is the difference in the K values determined from the red and blue narrow lines (there is no overlap in wavelength between these spectra), a difference well outside the errors in the line measurements and clearly obvious from the plot of fit radial velocities in Fig. 4. The wavelength calibration was checked by repeating the calibration procedure using FIGARO procedures. Although differences for a few individual blue spectra of up to 13 km s^{-1} were found using a number of combinations of line fit orders and line lists, no systematic differences with phase for either red or blue spectra were found. We checked for the effects of refraction, but no correlations between altitude, counts in the spectra or radial velocity that would suggest such had occurred were found. We checked the red- and blue-arm line velocities for two other stars observed during the same run – a flux standard and EC 11575−1845 – and we found no offset between their red and blue spectra. Finally, we measured the velocities for about 20 lines on the lower-resolution line-map spectra of V664 Cas, which were not used in the radial velocity study and were reduced separately. Although of limited phase coverage, the red (blue) lines fit well to the orbits determined from the red (blue) radial velocity spectra.

It could be that this effect is caused by overlap between spectral lines arising from other sources, i.e. from the primary star or absorption lines from the secondary star. The modified template spectra (Section 4.1) showed that all but one of the measured emission lines on the red spectra are likely to be affected, to any degree, by absorption lines from the secondary star. This is also unlikely for the primary star, as the only significant lines for this hot star (Section 6.2) in the red spectral region are Hα and He II. Lines from the primary star in the blue spectral region are a more likely contaminant, e.g. at C IV around 4650–4660 Å and He II 4686 Å. However, these lines are usually only significant in metal-rich or H-poor stars, neither of which we see any indications of. In addition, the $\Phi = 0$ spectrum of V664 Cas does not show any lines from the primary star other than H and He; at this phase, all lines from the primary star are at their strongest. Neither are any wind emission lines to be seen from the primary star.

However, if only one of the spectral data sets is correct in the K values measured, we would favour the red, as the blue spectra of night 2 had some problems. In addition, our red K values agree with those of Shimanskii et al. (2004), who measured ∼49 km s^{-1} for lines from 3900–5100 Å.[4]

The K value measured from the He II emission from the primary star was derived from Gaussian fit to a residual profile (Section 3.1). Note that the recovered profile is not, in fact, a Gaussian; it is instead only the part of the emission line that is not obscured by the emission from the irradiated secondary star. We estimate that fitting the residuals as we have, will result at most in an overestimate of the radial velocity of ∼25 km s^{-1} at phases 0.25 and 0.75; its value lies therefore between 49 and 74 km s^{-1}. However, if the blue spectra are wrong and we have measured the incorrect value of the radial velocities for the secondary star, then we would have also for the primary star from its He II line. Assuming that the same correction (but in the opposite direction, as the star moves in antiphase) can be applied, this would increase the K value for the primary star by about 15 km s^{-1}, its range then being from 64 to 89 km s^{-1}.

5.2 EC 11575–1845

For this system, we draw attention to the large difference in the K values for the H I emission lines and all others. Fig. 6 shows the spectra around $\Phi = 0.25$ and 0.75 for Hγ, showing the opposite symmetry of the profile at these phases; i.e. the absorption line is on the red side at phases around 0.25 and the blue side at phases around 0.75, implying that the absorption profile moves with a smaller overall radial velocity than the emission profile. However, the absorption component is likely to be from the same irradiated gas that gives rise to the emission component (Barman, private communication; see also Barman et al. 2004), being a reversal due to non-local thermodynamic equilibrium (NLTE) conditions. It should therefore be centred at the same wavelength. The fact that the H I profiles for EC

[4] The value they report is 49 km s^{-1}; however, this includes a correction, which appears to be about 9 km s^{-1}, designed to reflect the difference between the centre of mass and centre of light. If their value of 49 km s^{-1} is a measure of the centre of mass of the secondary star, it is then very different to our directly measured value.

11575−1845 are asymmetric (Fig. 2) may, in this case, arise not from differences to the velocities but rather from an asymmetrical nature to the emission component at phases around 0.25 and 0.75. If, at these phases, part of the irradiated face is 'eclipsed' (i.e. it is behind the star as viewed by us), then the equivalent parts of the H I profiles will not be seen. It would be necessary for the red parts of the emission line to be eclipsed when the star is moving towards us, for the line profile variations to be explained.

The H I line profile is rather complex, with flux (height and FWHM) varying with phase. With no flux calibration performed, we cannot disentangle the changes to the continuum level from those to the line fluxes. There is therefore considerable degeneracy in our fits, as the FWHM, radial velocity and line height can all vary – this for two Gaussian profiles of emission and one of absorption. To recover the radial velocity of the absorption component is not a problem, as this line is clearly seen and easy to fit for its trough. However, it is not possible to reliably measure the degree to which the H I profiles (their fluxes and FWHM) are affected by this suggested 'eclipsing'. However, to test whether our suggestion can at least approximately fit the data, we performed additional fits to the lines of H I 4340 Å. The (combined) line profile at $\Phi = 0.5$, with the emission and absorption components fixed to the same radial velocity, was used as a template for the spectral fits at phases from 0.21 to 0.81. The radial velocity and height of the three Gaussian components (two emission and one absorption), and to a lesser degree also the FWHM, were manipulated to find the best fits; this was defined by eye from the absorption component and the unaffected side of the emission component. A simple sine fit to these data gives a K value of about 118 km s^{-1}, very similar to the values obtained from the other lines on the spectra.

Not included in our measurements were the two ISIS spectra of EC 11575−1845. At their phases (0.18, 0.23), these look the same as the EMMI spectra, and have allowed us additionally to measure a radial velocity for He I 6678 Å of ∼20–30 km s^{-1} faster than the other emission lines at these phases.

5.3 Light curve

The light curves of V664 Cas in the V and I bands are shown in Fig. 7 in differential magnitudes such that the system is brightest at $\Phi = 0.5$. A double cosine (with least-squares minimization), mimicking a reflection plus ellipsoidal variation, gave the best fit to the data

$$A + B\cos\theta + C\cos 2\theta$$

where B is the flux semi-amplitude, A is the mean value and C/A is ∼4 per cent. We obtained from this the ephemeris T_0(HJD) = 244 9664.798(1) + 0.5817(2)E d, the period being that used in the radial velocity study and T_0 being within 0.025 ± 0.015 d of that from the spectral study. Our period is the same as that reported by Grauer et al. (1987) and Shimanskii et al. (2004).

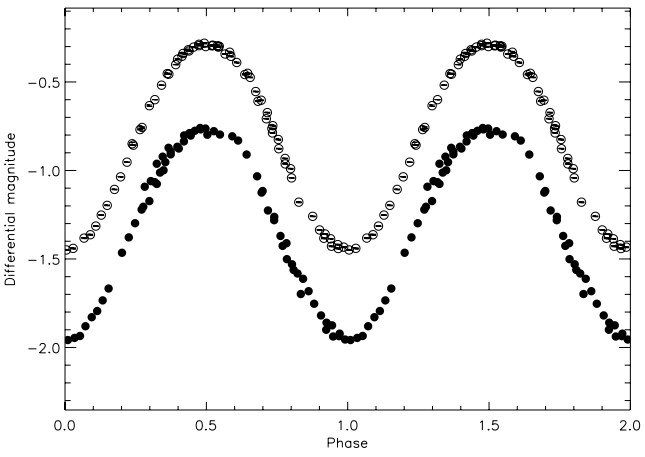

Figure 7. The I-band (filled symbols) and V-band (unfilled symbols) light curves for V664 Cas, plotted in differential magnitudes such that the system is brightest at $\Phi = 0.5$.

6 PARAMETERS OF THE PRIMARY STAR

6.1 EC 11575–1845

We estimated the effective temperature and surface gravity of the hot component of EC 11575−1845 using a model atmosphere analysis of a spectrum taken at $\Phi = 0.002$ when the contamination from the cool component is at a minimum.

A grid of hydrogen and helium composed model atmospheres were computed with the NLTE code developed by Werner (1986). Basic assumptions are those of static, plane-parallel atmospheres in hydrostatic equilibrium. As described by Werner, the accelerated lambda iteration method is used to solve the set of non-linear equations. Line blanketing by the Stark broadened lines of hydrogen and He II is taken into account self-consistently. Synthetic spectra are computed with detailed broadening tables. Details are provided in Napiwotzki (1997).

As a result of the lack of other temperature indicators, both effective temperature and gravity must be determined from the Balmer lines Hβ and Hγ present in the observed spectra. The line fits were performed with a modified version of the least-squares algorithm described in Bergeron, Saffer & Liebert (1992). The fit procedure is described in Napiwotzki (1999).

A simultaneous fit of the complete profiles of the Balmer and He II lines yielded $T_{\rm eff} = 120\,000$ K, $\log g = 6.6$ and $\log n_{\rm He}/n_{\rm H} = -0.9$, i.e. the helium abundance is close to the solar value. However, a closer look reveals that some contamination from the cool companion is still present. A very low level of emission from the secondary may still be present in the core of Hβ, and it is most likely that the emission core of He II 4686 Å also contains some additional contribution. Thus, we repeated the fit with the line cores (±3 Å) excluded. The resulting parameters are $T_{\rm eff} = 105\,000$ K, $\log g = 6.7$ and $\log n_{\rm He}/n_{\rm H} = -0.8$. We must also be aware of continuum light of the cool companion, which may contribute to the spectrum. We tested the possible influence on our parameter determination by artificially subtracting a constant amounting to 20 per cent of the spectral continuum, thus increasing the line depths. Fits of this spectrum yielded $T_{\rm eff} = 86\,000$ K, $\log g = 6.8$, $\log n_{\rm He}/n_{\rm H} = -0.9$ (line cores excluded) and $T_{\rm eff} = 117\,000$ K, $\log g = 6.3$, $\log n_{\rm He}/n_{\rm H} = -0.9$ (line cores included). Because the fit of the 20 per cent continuum subtracted spectrum is significantly worse than the fit of the original spectrum, we very likely overestimated the possible contribution of the companion to the continuum. We conclude that the fit of the original spectrum without the line cores gives the most reliable parameters and we estimate conservative error limits from our different fit approaches: $T_{\rm eff} = 105\,000 \pm 20\,000$ K, $\log g = 6.7 \pm 0.3$ and $\log n_{\rm He}/n_{\rm H} = -0.8 \pm 0.1$. The fits are shown in Fig. 8.

These parameters place the sdO component of EC 11575−1845 in the Hertzsprung–Russell diagram in the region occupied by the central stars of old PNe analysed by Napiwotzki (1999). However, to our knowledge, no PN around EC 11575−1845 has been detected.

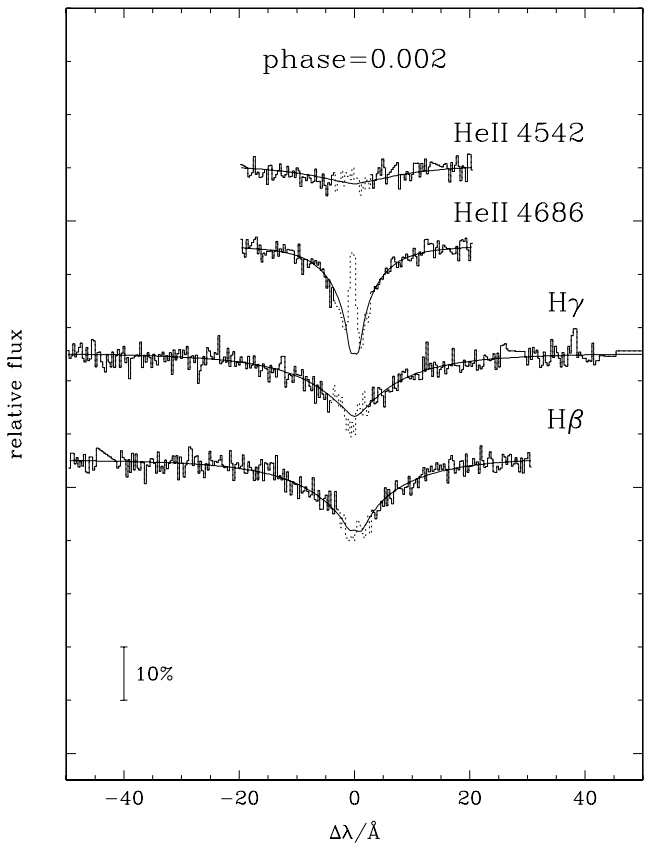

Figure 8. The spectra and fits to the $\Phi \sim 0$ spectra of EC 11575−1845, with the core of the profile not included in the fits.

According to the post-AGB tracks for single H-rich stars from Blöcker (1995), Schönberner (1983) and Koester & Schönberner (1986), as compiled in Napiwotzki (1999), these stellar parameters correspond to a mass range 0.547–0.605 $M_\odot$. A slightly lower mass results from comparison to the post-early-AGB track.

EC 11575−1845 has no detected nebula, but we estimated the expansion time-scale of the nebula following Mendez et al. (1988), who searched for PNe around hot sdO stars

$$t = 2.57 \times 10^3 M_{\rm neb}^{0.4} ({\rm EM})^{-0.2} v_{\rm exp}^{-1}$$

with values and units as follows. The emission measure (EM), calculated from the lack of nebula, is <30 cm^{-6} pc (we assumed the same limit for the Digitized Sky Survey as for the Palomar Sky Survey) and $v_{\rm exp} = 20$ km s^{-1} (assumed). For the ionized mass of the nebula we adopted not the Mendez et al. value of 0.5 $M_\odot$, but a smaller value of 0.1 $M_\odot$. This is based on the low ionized nebular masses found for the similar binary PN central stars UU Sge and V477 Lyr (Bell et al. 1994). This results in a date for nebular ejection of $>25\,000$ yr ago. Compare this to the time-scale (taken from the evolutionary models cited in this section) for the star to reach its current state: 360 000, 220 000 and 7250 yr for 0.546-, 0.565- and 0.605-$M_\odot$, stars, respectively. These time-scales are very sensitive to the mass; however, it seems likely that the higher-mass possibility of these three is eliminated.

6.1.1 Balmer line 'problem'

Napiwotzki & Rauch (1994) reported on the so-called Balmer line problem for stars with parameters similar to EC 11575−1845: model atmosphere fits to different Balmer lines yielded discrepant temperature estimates, with higher Balmer lines yielding systematically higher values. Several lines of evidence indicate that the higher temperature derived from Hδ/Hϵ is close to the real value (Napiwotzki 1999). Werner (1996) has shown that by including the elements C, N and O in the atmospheric calculations, a detailed treatment of their line opacities, and their impact on the atmospheric temperature structure, can resolve the discrepancy for the sdO star BD+28 4211 ($T_{\rm eff} = 82\,000$ K). This does not work as well for hotter central stars, the most probable reason being still missing opacity from other elements and/or lines.

Computation of a grid of models of the type presented in Werner (1986) is time-consuming and the results would depend on the adopted metallicity (which we cannot accurately measure for EC 11575−1845). For our analysis, because only the Balmer lines Hβ and Hγ were available, we have to be aware that the real temperature of EC 11575−1845 is probably higher than 105 000 K. A comparison with the central star analysis of Napiwotzki (1999) indicates that this effect is typically of the order of 15 000 to 20 000 K, although it can be significantly smaller; this is within our error estimates.

6.2 V664 Cas

For V664 Cas, *IUE* ultraviolet spectra were studied by Heckathorn & Fesen (1985). From the featureless continuum they derive a blackbody temperature of 50 000–60 000 K, but with an allowed range of 35 000–120 000 K. An unpublished light-curve analysis by Malasan & Yamasaki resulted in a temperature of $\sim$100 000 K, and the more detailed modelling of Shimanskii et al. (2004) suggests a value of 83 000 $\pm$ 6000 K. The appearance of the emission core of He II supports this higher temperature. Although the strength of this feature is also dependent on other parameters, e.g. metallicity and surface gravity, of the sample of PN central star spectra in Napiwotzki (1999), those with emission in the core (either on the model or actual spectrum) tend to be of $T_{\rm eff} > 100\,000$ K, while those without are of lower temperatures (down to 35 000 K). The helium abundance also plays a role in determining the emission core, but for the younger PN central stars on the horizontal part of the Hertzsprung–Russell diagram, it is less important for older stars such as V664 Cas.'

A lower limit on the primary mass can be placed by consulting the theory of PN central stars. At $M < 0.3$–0.4 $M_\odot$, the primary star of V664 Cas would not become hot enough within the lifetime of its nebula (normally a few $\times 10^4$ yr) to excite the hydrogen (Iben & Tutukov 1993; Yungelson, Tutukov & Livio 1993). In addition, stars of mass less than about 0.5 $M_\odot$ are not expected to ever reach a $T_{\rm eff}$ of 100 000 K (e.g. see the evolutionary tracks mentioned previously). The upper mass limit for the primary of V664 Cas is set only by the condition not to be greater than the Chandrasekhar mass. However, if $T_{\rm eff} \sim 100\,000$ K, the evolutionary time-scale for a high-mass primary would be so fast that the nebula found around it, while still in its high-temperature phase, would be small and young, whereas HFG 1 has the properties of an evolved nebula (Heckathorn, Fesen & Gull 1982).

7 SOME SYSTEM PARAMETERS

Kepler's laws allow us to use measured K values to calculate, as a function of inclination, the mass of the stars and their semimajor axis (distance to the centre of mass of the system)

$$M_{\rm p,s} \sin^3 i = 1.0361 \times 10^{-7} (K_{\rm p} + K_{\rm s})^2 K_{\rm s,p} P \ {\rm M}_\odot \quad (1)$$

$$a_{\rm p,s} \sin i = 1.9758 \times 10^{-2} K_{\rm p,s} P \ {\rm R}_\odot \quad (2)$$

Table 2. Some derived parameters for V664 Cas and EC 11575−1845, in solar units. Only the values in the favoured range (see text) are given. Subscripts are as follows: 'p' refers to the primary star, 's' to the secondary star, 'rl' to the Roche lobe radius of the secondary star, and 'rem' to the red emission lines. *R* are radii, *i* inclination, *M* mass and *a* the semimajor axes.

i	M_p	M_s	a_p	a_s	R_{rl}	R_{rem}	R_p
			V664 Cas				
$K_p = 89$ km s^{-1}							
27	1.3	1.6	2.2	1.9	1.6	0.76	
33	0.77	0.90	1.9	1.6	1.4	0.63	
43	0.39	0.46	1.5	1.3	1.1	0.51	
$K_p = 74$ km s^{-1}							
25	1.4	1.3	2.0	2.1	1.5	0.81	
31	0.75	0.73	1.6	1.7	1.3	0.67	
39	0.41	0.40	1.4	1.4	1.0	0.55	
$K_p = 49$ km s^{-1}							
21	1.6	1.0	1.6	2.4	1.4	0.96	
29	0.63	0.41	.2	1.8	1.0	0.71	
35	0.38	0.24	0.98	1.5	0.86	0.60	
			EC 11575−1845				
$K_s = 125$ km s^{-1}							
37	0.61	0.26	0.56	1.3	0.55		0.058
41	0.47	0.20	0.52	1.2	0.5		0.051
$K_s = 185$ km s^{-1}							
55	0.64	0.18	0.41	1.5	0.49		0.059
59	0.56	0.16	0.39	1.4	0.47		0.055
65	0.48	0.13	0.37	1.3	0.45		0.051

where $K_{p,s}$ are the K values for the centre of mass of the primary and secondary stars and units are solar (mass, radius), km s^{-1} (velocity) and d (period). The Roche lobe radius (R_L) can be calculated from the mass ratio ($q = M_p/M_s$ for the primary star radius, and vice versa), using

$$r_L = \frac{0.49q^{2/3}}{0.6q^{2/3} + \ln(1 + q^{1/3})}$$

(Eggleton 1983) where $r_L = R_L/a$.

Although we do not have a full complement of measured K values for our two systems, none the less it is instructive to compute the range of masses for their individual components, as a function of inclination. These are given in Table 2. For V664 Cas, three sets of calculations are presented, covering the range of possible values for K_p (49, 74 and 89 km s^{-1}).[5] For this object, we also have measured values of K_s. For EC 11575−1845 we have a measured value for K_p, and we present two sets of calculations made with $K_s = 125$ and 185 km s^{-1}. The former is the value measured for the centre of light of the irradiated surface from the narrow emission lines, and the latter is an upper limit based on the fact that at this velocity, the centre of light of the emission lines is almost coincident with the Roche lobe radius. In addition, Table 2 gives the semimajor axis values and the Roche lobe radius for the secondary star, the radius of the primary star of EC 11575−1845 and the radius of the centre of light of the red emission lines of V664 Cas. These radii values were calculated with equation (2) using the K values for the emission lines, subtracting then from a_s the a_{em} thus determined.

[5] To summarize, 49 km s^{-1} is the lower limit assuming that the blue spectra have not been corrupted, and 74 km s^{-1} is the measured value assuming the same. 64 km s^{-1} is the lower limit assuming the blue spectra have been corrupted, and 89 km s^{-1} is then the 'measured' value. We have not carried out separate calculations for 64 km s^{-1} as these are close to those for 74 km s^{-1}.

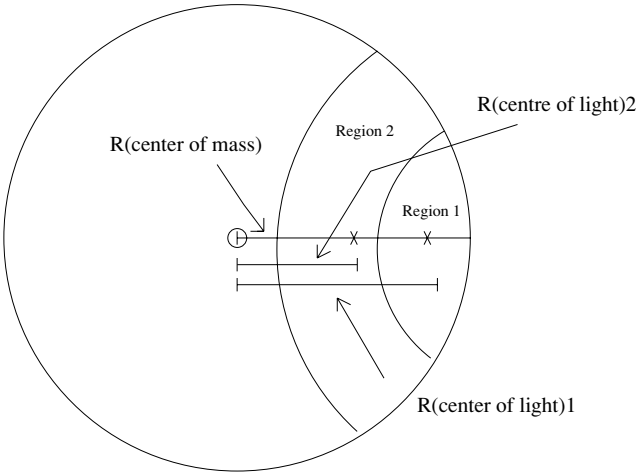

Figure 9. Explanation of the centre of mass versus centre of light. The primary star is located to the right, off-plot, as is also the centre of mass of the binary system. K values increase as one moves outwards toward the left. R is the radius of the star, and emission lines distributed evenly about this point will measure the motion of the centre of mass (i.e. the centre of the star). Emission lines arising from a specific location only (e.g. the irradiated surface) will measure the motion of the centre of light of that region, in this case producing K values that are less than those from the centre of mass of the star. As calculated here, a larger irradiated spot (region 2) will have a radius (counting from the centre of the star outwards) of a smaller value than will a small irradiated spot (region 1).

Large values mean a small 'hotspot' (see Fig. 9 for a more detailed explanation). The blue emission lines, having a higher measured K value, would have smaller radius values at each inclination, and thus a larger hotspot.

We have limited the entries of Table 2 to within the ranges that correspond to the limits for the masses of the primary stars, following the discussion in Section 6. The values in Table 2 are to indicate how the system parameters depend on the inclination, rather than for the reader to use the values for any subsequent analysis (as at present there are still too many unknowns). For EC 11575−1845, we suggest that the primary mass lies between about 0.5 and 0.6 $M_\odot$. For V664 Cas, a lower limit to the primary star's mass of 0.4 $M_\odot$ is probably conservative. The upper limit to the spectral type for the secondary star (and thus its and the primary star's masses) is not useful here, as the Chandrasekhar mass for the primary star (1.44 $M_\odot$) is reached first.

For EC 11575−1845, the secondary star is always of very low mass, while for V664 Cas it is more massive; indeed, for the fastest K_p value, the secondary is more massive than the primary star. This was also claimed by Shimanskii et al. (2004), and is very rare for these PCEBs, as also discussed by Exter, Pollacco & Bell (2004) in their study of VW Pyx. In addition, the size of the irradiated surface for V664 Cas is probably quite small.

The radius of the primary star of EC 11575−1845 was calculated from the mass and the value of log g calculated from the model fit of Section 6. These values are just larger than a typical white dwarf radius, e.g. 0.017–0.012 $R_\odot$ for a 0.3–0.6 $M_\odot$ white dwarf using the Nauenberg formula (Nauenberg 1972); these are lower limits as this relation assumes zero temperature and no rotation.

8 STARK BROADENING

Both binary systems have very broad H I emission lines. If the H I lines are formed on or near the heated hemisphere, it is instructive

to estimate the physical conditions under which they are formed. Assuming $T_{\rm p} \sim 10^5$ K, $R_{\rm p} \sim 0.1$ R$_\odot$ for the primary and a solar-sized secondary orbiting three radii distant, then the fraction

$$\frac{R_{\rm s}^2\theta^2}{4(a-R_{\rm s})^2}$$

of the flux is intercepted by the secondary. Here θ is the approximate opening angle viewed from the centre of the secondary over which heating takes effect. Assuming the flux from the heated surface of the secondary is the dominant source from this body, then

$$\frac{R_{\rm s}^2\theta^2}{4(a-R_{\rm s})^2}L_{\rm p} = L_{\rm s} = \pi R_{\rm s}^2\theta^2\sigma T_{\rm s}^4$$

and therefore

$$T_{\rm s} = T_{\rm p}\left(\frac{R_{\rm p}}{a-R_{\rm s}}\right)^{0.5},$$

leading to a maximum value $T_{\rm s} \sim 22\,000$ K at the substellar point. Using our low-resolution spectra of V664 Cas, we estimate the density in the formation region from the relation given by Inglis & Teller (1939), which is based on the highest line in the Balmer sequence that is detected (13). This leads to a (positive) ion density of $\sim 8 \times 10^{14}$ cm^{-3}.

These values are similar to those seen in B stars, suggesting that Stark broadening will be significant. Stehlé & Hutcheon (1999) presented tables of Stark and Doppler broadened hydrogen line profiles over a large range in plasma temperature and density. While direct comparison with our hydrogen line profiles is complicated by the presence of the central absorption, tests with suitably scaled Stehlé & Hutcheon profiles at the gas conditions given above do resemble those observed. For both systems, however, a further narrow component is required to match the expected core intensity.

9 DISCUSSION

Very little detailed previous work had been done on the components of V664 Cas until the work of Shimanskii et al. (2004). They fitted their light curves and spectra with an irradiation model (although they do not go into full detail of these models), but, with lower-resolution spectra than ours, could not follow in as much detail the behaviour of the various line profiles with phase. They did find that V664 Cas is likely to be a system with a massive secondary star, exceeding that of the primary star by a factor of 1.6. We can confirm that this certainly is a possibility. Acker & Stenholm (1990) commented on the apparent similarity of its emission-line spectrum to those of some polars, where the emission is formed in an accretion column falling on to the white dwarf. However, there is currently no reported evidence for rapid variability in the light curves (those cited in Section 1 and ours) or spectra that may be associated with an accretion disc. Chen et al. (1995) carried out the first detailed study of EC 11575−1845. From medium-resolution spectra, they found $K_{\rm p} = 40$ and $K_{\rm irr} = 119$ km s^{-1}, similar to our values, and the range of masses we suggest for the components of this system agrees broadly with that which they derive from their favoured light-curve solutions.

Our phase-resolved resolution spectra of both binary systems reveal a rich emission-line spectrum arising from the irradiated surface of the secondary star. Lines of H I, He I,II and narrower lines of C, N and O were found, as well as Stark broadened H I profiles with absorption components – possibly due to NLTE conditions in the irradiated gas – superimposed. The H I emission and absorption lines of EC 11575−1845 have different measured K values, which we suggest could be due to the emission lines being intrinsically asymmetrical at phases around 0.25 and 0.75, where part of the irradiated face will be hidden from view. For V664 Cas, the H I absorption profile appears to double for Hα at phases around 0. To check the possibility that this second profile arises from the photosphere from the secondary star, we summed together a fit to the Hα emission + single absorption profile at $\Phi = 0$, with the diluted template spectra (Section 4). Within our preferred range of spectral type, there is sufficient flux at Hα to be seen against the emission line; however, the template lines are much wider that the observed absorption profile.

By considering the limits set to the masses of the primary stars for both systems, we can set limits to their inclinations. For EC 11575−1845, the mass limits of 0.55–0.61 M$_\odot$ (the upper end being less likely) lead to inclinations of 37°–40° to 57°–62° for the upper and lower limits to $K_{\rm s}$, respectively. These lead to a secondary star mass <0.3 M$_\odot$. For V664 Cas, we only have a lower limit to the primary star mass, of about 0.5 M$_\odot$. The inclination will lie somewhere between 20° and 40°, for the full range of $K_{\rm p}$ adopted. This agrees with the suggested 30° inclination for V664 Cas found by Pigulski & Michalska (2002) from an incomplete light curve. An upper limit to the mass can be placed at 0.6 M$_\odot$ or so, based on the fact that the nebula around the PN may be >25 000 yr, assuming the star has evolved in the same way as the theoretical models cited in Section 6.

There is one system that, spectroscopically, is very similar to ours: BE UMa. BE UMa has a large reflection effect (1.5 mag; Kurochkin 1964, 1971) with partial eclipses. The emission-line spectrum of Ferguson & James (1994) is very similar to ours, although with stronger He II 4686 Å relative to the 4640-Å complex, and narrower H I profiles. They noted that Hβ and He II lines have absorption cores at $\Phi = 0.84$ and 0.15, but did not plot the spectra to show this. The parameters of the sdO primary, $T_{\rm eff} = 105\,000$ K and $\log g = 6.5$ (Liebert et al. 1995), are very similar to those for EC 11575−1845, although the period of the system is much longer, 2.29 d, with separation of 7.5 R$_\odot$. However, these authors concluded a high mass, 0.7 M$_\odot$ for the primary and 0.36 M$_\odot$ for the secondary, based on the results from a radial velocity study, claiming $T_{\rm eff}$ measured from the Balmer lines was in fact too low.

There exists some indirect evidence that the mass of BE UMa is however at the lower end of their quoted error range. Ferguson & James (1994) used the formalism developed by Iben & Tutukov (1993) to estimate the mass of the sdO progenitor. The result was an original mass of 3–4 M$_\odot$, which would indicate that BE UMa is a member of the young disc population. However, BE UMa has a high galactic latitude, and with the distance of 1.9 kpc calculated by Liebert et al., it would be 1.7 kpc away from the galactic plane. Clearly this is at odds with membership of the young disc population, but consistent with old disc population membership. Furthermore, the nebula around BE UMa is already old and faint (they estimated a kinematical age of 40 000 yr). A 0.7-M$_\odot$, post-AGB star would evolve too fast according to the evolutionary calculations (Schönberner 1993; Blöcker 1995) and we would expect a much younger, brighter PN.

The only other PCEB system with such a rich emission-line spectrum is VW Pyx, which unfortunately is also quite faint. Exter et al. (2004) obtained limits to the mass ratio (suggesting that, unusually, the primary star may be less massive than the secondary) and studied the bipolar 'jets' of the inner (planetary) nebula. The PCEBs UU Sge and V477 Lyr are also similar to our two systems, with broadly similar masses (∼0.5–0.6 M$_\odot$ for the primary stars and 0.3 M$_\odot$ for the secondary stars, similar at least to EC 11575−1845) and orbital periods ($P \sim 11$ h). Their emission-line spectra are not as rich or

strong as are ours, although they do show the lines around 4645 Å, and the spectrum of the primary star is much more prominent. This latter is possibly due to the larger radius (and thus luminosity) of the primary stars, being about 0.2–0.3 $R_{\odot}$, compared to a value likely to be <0.06 $R_{\odot}$ for EC 11575−1845. As the primary stars have similarly high temperatures (at or above 60 000 K; Bell et al. 1994; Pollacco & Bell 1994), the difference in the emission-line spectrum (both the number of lines and their strengths) will provide, together with our two systems, interesting constraints on models of the irradiation in these hot PCEBs, especially on the relative importance of the radii, inclination and separation.

The distances derived by Bell et al. (1994) and Pollacco & Bell (1994) for UU Sge and V477 Lyr (2.4 and 1.7 kpc) suggest ionized diameters of the central low surface brightness nebula of >0.5 pc (in the case of UU Sgr associated material has been found more than 2 pc from the star; Pollacco & Bell 1997). Assuming a linear expansion rate of 20 km s^{-1} leads to ages $>23\,000$ yr – old by PN standards. However, the central stars have radii and luminosities consistent with sdO stars, while EC 11575−1845 appears to have evolved further along towards a white dwarf status. For UU Sge and V477 Lyr, it is suggested that the primary star has influenced the evolution of the secondary star, particularly witnessed by the over-large radius for their mass values. It would be interesting therefore to obtain values for the radii of the secondary stars for V664 Cas and EC 11575−1845.

There are many other irradiated stellar systems, from PCEBs to X-ray binaries and cataclysmic variables. The physics of the irradiation of the secondary star in some PCEBs has been modelled by Barman et al. (2004), as mentioned in Section 1. UU Sge and AA Dor are their examples of extreme irradiated systems, with large and hot primary stars. For UU Sge, they model a maximum temperature in the heated region of 40 000 K and for AA Dor 33 000 K; compare this to the intrinsic temperature of the secondary stars of 6250 and 3000 K, respectively. This shows the enormous effect the irradiation has on these secondary stars. Irradiation effects are also seen in cooler white dwarf binaries. In these systems, the primary component's radiation field is considerably softer than in the systems considered here. In many systems, this manifests itself as a weak reflection effect with an absorption-line spectrum with a weak Hα emission component (e.g. PG 0308+096; Saffer et al. 1993), while in others no emission components at all are detectable (e.g. HW Vir; Wood & Saffer 1999). Other factors, such as the size of the secondary (and its unirradiated temperature), also influence the emission-line formation. In the case of the totally eclipsing system NN Ser ($P \sim 0.13$ d), phase-dependent absorption and emission components have been detected (Catalán et al. 1994; Haefner et al. 2004), leading to component masses similar to those presented here (0.54 and 0.15 $M_{\odot}$, respectively).

ACKNOWLEDGMENTS

We thank Tom Marsh for PAMELA and MOLLY, Harry Shipmen for advice on the Stark broadening calculation, and Barrey Smalley, Darko Jevremovic and especially Yvonne Unruh for their advice. We used SIMBAD, maintained by the Centre de Données astronomiques de Strasbourg, and the National Aeronautics and Space Administration (NASA) Astrophysics Data System. Some of the data presented in this paper were obtained from MAST. The Space Telescope Science Institute is operated by the Association of Universities for Research in Astronomy, Inc., under NASA contract NAS5-26555. Support for MAST for non-*Hubble Space Telescope* data is provided by the NASA Office of Space Science via grant NAG5-7584, and by other grants and contracts. The Digitized Sky Surveys were produced at the Space Telescope Science Institute under US Government grant NAG W-2166. The images of these surveys are based on photographic data obtained using the Oschin Schmidt Telescope on Palomar Mountain and the UK Schmidt Telescope. The plates were processed into the present compressed digital form with the permission of these institutions. This work is based on observations made with the WHT and JKT operated on the island of La Palma by the Isaac Newton Group in the Spanish Observatorio del Roque de los Muchachos of the Instituto de Astrofísica de Canarias.

REFERENCES

Acker A., Stenholm B., 1990, A&A, 233, L21
Acker A., Ochsenbein F., Stenholm B., Tylenda R., Marcout J., Schohn C., 1992, Strasbourg–ESO Catalogue of Galactic Planetary Nebulae. European Southern Observatory
Barman T. S., 2002, Irradiated model atmospheres for extrasolar giant planets and secondary stars of pre-cataclysmic variables, PhD thesis. University of Georgia, USA
Barman T. S., Hauschildt P. H., Allard F., 2004, ApJ, 614, 338
Beer M. E., Podsiadlowski P., 2002, MNRAS, 335, 358
Bell S. A., Pollacco D. L., Hilditch R. W., 1994, MNRAS, 270, 449
Bergeron P., Saffer R. A., Liebert J., 1992, ApJ, 394, 228
Blöcker T., 1995, A&A, 299, 755
Bond H. E., 2000, in Kastner J. H., Soker N., Rappaport S. A., eds, Asymmetrical Planetary Nebulae II: From Origins to Microstructures. Astron. Soc. Pac., San Francisco, p. 115
Catalán M. S., Davey S. C., Sarna M. J., Connon Smith R., Wood J. H., 1994, MNRAS, 269, 879
Chen A., O'Donoghue D., Stobie R. S., Kilkenny D., Roberts G., van Wyk F., 1995, MNRAS, 275, 100
Drilling J. S., 1985, ApJ, 294, L107
Eggleton P. P., 1983, ApJ, 268, 368
Exter K. M., Pollacco D. L., Bell S. A., 2004, MNRAS, 341, 1349
Exter K. M., Barman T. S., Pustynski V.-V., Pollacco D. L., Bell S. A., Pustylnik I., 2005, in Proceedings of Interacting Binaries. American Institute of Physics, New York, in press
Ferguson D. H., James T. A., 1994, ApJS, 94, 723
Ferland G. J., 1991, Ohio State Univ. Internal Report 91-01
Grauer A. D., Bond H. E., Ciardullo R., Fleming T. A., 1987, BAAS, 19, 643
Haefner R., Fiedler A., Butler K., Barwig H., 2004, A&A, 428, 181
Heckathorn J. N., Fesen R. A., Gull T. R., 1982, A&A, 114, 414
Iben I. Jr, Livio M., 1993, PASP, 105, 1373
Iben I. Jr, Tutukov A. V., 1993, ApJ, 418, 343
Inglis D. R., Teller E., 1939, ApJ, 90, 439
Jenniskens P., Desert F.-X., 1994, AAS, 106, 39
Koester D., Schönberner D., 1986, A&A, 154, 125
Kurochkin N. E., 1964, Peremnye Zvezdy (Academy Sci. USSR Var. Star Bull.), 15(1), 77
Kurochkin N. E., 1971, Peremnye Zvezdy (Academy Sci. USSR Var. Star Bull.), 18, 85
Liebert J., Tweedy R. W., Napiwotzki R., Fulbright M. S., 1995, ApJ, 441, 424
Mastrodemos N., Morris M., 1999, ApJ, 523, 357
Mendez R. H., Gathier R., Simon K. P., Kwitter K. B., 1988, A&A, 198, 287
Montes D., Ramsey L. W., Welty A. D., 1999, ApJS, 123, 283
Napiwotzki R., 1997, A&A, 322, 256
Napiwotzki R., 1999, A&A, 350, 101
Napiwotzki R., Rauch T., 1994, A&A, 285, 603
Nauenberg M., 1972, ApJ, 175, 417
Pigulski A., Michalska G., 2002, IBVS, 5218, 1
Pollacco D. L., Bell S. A., 1993, MNRAS, 262, 377
Pollacco D. L., Bell S. A., 1994, MNRAS, 267, 452
Pollacco D. L., Bell S. A., 1997, MNRAS, 284, 32

Prugniel Ph., Soubiran C., 2001, A&A, 369, 1048
Pustylnik I., Pustynski V., Kubat J., 2001, Odessa Astronomical Publications, 14, 87
Rasio F. A., Livio M., 1996, ApJ, 471, 366
Saffer R. A., Wade R. A., Liebert J., Green R. F., Sion E. M., Bechtold J., Foss D., Kidder K., 1993, AJ, 105, 1945
Schönberner D., 1983, ApJ, 272, 708
Schönberner D., 1993, in Weinberger R., Acker A., eds, IAU Symp. 155, Planetary Nebulae. Kluwer, Dordrecht, p. 415
Seaton M. J., 1979, MNRAS, 187, 739
Shimanskii V. V., Borisov N. V., Sakhibullin N. A., Surkov A. E., Astron. Rep., 48, 563
Stehlé C., Hutcheon R., 1999, A&AS, 140, 93
Tody D., 1993, in Hanisch R. J., Brissenden R. J. V., Bartnes J., eds, ASP Conf. Ser. Vol. 52, IRAF in the Nineties: Astronomical Data Analysis Software and Systems II. Astron. Soc. Pac., San Francisco, p. 173
Werner K., 1986, A&A, 161, 177
Werner K., 1996, ApJ, 457, L39
Wood J. H., Saffer R., 1999, MNRAS, 305, 620
Yungelson L. R., Tutukov A. V., Livio M., 1993, ApJ, 418, 794

This paper has been typeset from a TEX/LATEX file prepared by the author.